



An Experimental and Analytical Study of Influential Parameters of Parabolic trough Solar Collector

Daryoosh Borzuei, Seyed Farhan Moosavian, Abolfazl Ahmadi*, Rouhollah Ahmadi*, Kourosh Bagherzadeh

School of New Technologies, Department of Energy Systems Engineering, Iran University of Science & Technology, Tehran, Tehran, Iran.

PAPER INFO

Paper history:

Received 14 December 2020
Accepted in revised form 17 August 2021

Keywords:

Solar Collector,
PTC,
Heat Transfer Fluid,
Vacuum Tube,
Analytical Study

ABSTRACT

Energy plays a vital role in all human life activities. Due to the problems caused by fossil fuels in recent decades such as global warming, greenhouse gas emissions, ozone depletion, etc., the use of renewable and clean energy has been considered. An experimental facility for the acquisition of reliable data from Parabolic Trough Solar Collectors (PTCs) was established to develop a robust analytical model. A wide range of Heat Transfer Fluid (HTF) flow rates (0.0372-0.1072 kg/s) and solar radiation (400-900 W/m²) were used to determine PTC parameters such as the outlet temperature of HTF loss and temperature distribution. Vacuum conditions in the receiver were considered effective in terms of thermal efficiency. Also, three types of HTF including two oil fluids (Syltherm 800 and S2) and water were examined. The temperature distribution showed that when Syltherm 800 or S2 passed through the absorber tube, the outlet temperature was higher than water: 2.84 % for Syltherm 800 and 3.72 % for S2. Since the absorber tube temperature was much higher than water, the heat loss in this condition was considered for oil HTF. Of note, the results demonstrated that use of the vacuum tube could diminish heat loss for the oil HTF. The effect of solar intensity increases from 600 W/m² to 900 W/m² on the maximum temperature of the receiver tube indicated that when Syltherm 800 was used as an HTF, this temperature increased by 35.1 % (from 167 °C to 219 °C), while this percentage was 32.7 % and 6.8 % for S2 and water, respectively.

<https://doi.org/10.30501/jree.2021.261647.1172>

1. INTRODUCTION

In current years, the development of energy consumption and the growing trend of using fossil fuels have led to widespread adverse environmental damage such as greenhouse gas emissions and global warming [1]. In order to overcome these problems, the use of renewable energy as a viable alternative to fossil fuels has led to the development of energy harvesting technologies from solar, wind, geothermal, hydroelectric, and biomass sources [2]. Meanwhile, due to the advantages of solar energy such as cleanliness, easy access, and greater sustainability, this energy has found a special place among renewable energy sources which have paid a great deal of attention to this area of research [3]. Solar radiation can be used for a variety of purposes such as generating power, providing heating and cooling loads, preparing fresh water for residential and industrial use, and air conditioning [4, 5]. In solar thermal collectors, generally, the temperature of the working fluid is raised through absorption of solar radiation and then, this heat is transferred to operating fluid [6].

In general, thermal solar collectors are segmented into two categories: flat and concentrated solar collectors [7]. In decentralized solar collectors, the output temperature range is

less than centralized solar collectors. Therefore, the concentrated solar collectors such as solar dishes and linear parabolic collectors (PTCs) are applicable since high temperatures are needed [8]. The temperature range for the PTC is in the range of 30 to 400 °C. This type of solar collector is capable of producing superheated steam for power generation in solar power plants [9-11]. Due to the role of solar collectors in supplying heat to residential and industrial places, many researches have been focused to increase the capacity factor, stability and efficiency [12]. These studies have been conducted in the form of numerical simulations and experimental tests to evaluate the effect of changing geometrical parameters of solar collectors, type of working fluid, geographic orientation and location, and other relevant parameters. The following is a review of some research in this area of study. Kalogirou [13] conducted a comprehensive overview of different kinds of solar collectors and their applications. In this regard, the performance of different types of solar collectors such as flat plate, compound parabolic, evacuated tube, parabolic lens, parabolic dish, and heliostat was examined from the thermal, optical, and thermodynamic points of view.

Some numerical studies have provided information related to the geometry and the use of linear parabolic collector tube feeders. In this regard, Bellos et al. [14] studied different arrangements of fins in the absorber tube of LS-2 linear parabolic collectors by numerical modeling. They examined

*Corresponding Author's Email: a_ahmadi@iust.ac.ir (A. Ahmadi) and ahmadi@iust.ac.ir (R. Ahmadi)
URL: https://www.jree.ir/article_135327.html

Please cite this article as: Borzuei, D., Moosavian, S.F., Ahmadi, A., Ahmadi, R. and Bagherzadeh, K., "An experimental and analytical study of influential parameters of parabolic trough solar collector", *Journal of Renewable Energy and Environment (JREE)*, Vol. 8, No. 4, (2021), 52-66. (<https://doi.org/10.30501/jree.2021.261647.1172>).



twelve different fins with different lengths and thicknesses for linear parabolic collectors. The result showed that increasing the absorber length caused an increase in fluid temperature on the one side, and an increase in pressure drop, on the other side. Bellos et al. [15] did not consider this point of view, i.e., the examination of star fins on the absorber tube of the solar parabolic collector was carried out. Some researchers have studied the effect of fin geometry inside of the absorber tube of the solar collector from the numerical and experimental points of view. In this respect, Xiao et al. [16] analyzed the theoretical and empirical effects of using rectangular fins inside of the absorber tube of linear parabolic collectors. The results of this study showed that the rectangular shape of the inside absorber enhanced the performance of solar collectors.

Some studies have analyzed the effect of different types of working fluid inside the absorber tube on the performance of the PTC. Bellos and Tsivandis [17] investigated the effect of using hybrid nanofluid on the linear parabolic solar collectors. They modeled an LS-2 linear parabolic solar collector with Syltherm 800 oil as a working fluid in EES software. The results of this study showed that this hybrid nanofluid could enhance the thermal efficiency of the system by 1.8 %. Marefati et al. [7] analyzed the impact of different types of working fluid in the linear parabolic solar collector in different climates of Iran. The investigation of different types of working fluids on the performance of the thermal energy of solar collectors has also been the goal of some studies. Boukelia et al. [18] investigated the effect of two types of working fluids consisting of molten salt and thermal oils in solar collectors. The results demonstrated that the thermal efficiency of thermal oil as a working fluid in the solar collector was better than that of molten salt.

Studies on these topics have not been sufficient and there have been some numerical and experimental studies on the design and construction of linear parabolic collectors. In this regard, Dudley et al. [19] studied the efficiency and thermal loss of linear parabolic solar collector SEGS LS-2 by numerous experimental tests. They examined two different materials as an absorber tube in a linear parabolic solar collector. Reddy et al. [20] studied the effect of using porous

plates in an absorber tube of the linear parabolic solar collector with an area of 15 m². They studied the application of six different configurations of porous plates inside the absorber tube and it concluded that the use of a porous plate enhanced the performance of linear parabolic solar collectors.

This paper represents a comprehensive investigation of the impact of variation of solar radiation intensity and mass flow rate of working fluid on temperature changes of HTF in the parabolic solar collector. The results of this investigation have been obtained with an experimental test and a numerical simulation of a linear PTC modeled in MATLAB software. The obtained results of simulation and experiments are validated with each other. Investigation of three types of heat transfer fluids with eight different mass flow rates for changing solar radiation intensity is analyzed. Besides, the effect of the presence or absence of the vacuum in the space between the absorber tube and the coating on the heat transfer fluid temperature at different radiations was also investigated. Also, the temperature distribution across the collector was obtained for three types of heat transfer fluid by numerical simulation. The novelty of this research is in expressing the results in a new and tangible way using temperature and parametric distribution diagrams as a comparison criterion.

2. Experimental Description

2.1. Typical parabolic trough collector

A test facility composed of a PTC is made, as shown in Figure 1 and a black-coated copper tube is enclosed in a Pyrex glass tube located at the focal line of the parabolic mirror as a solar collector receiver. Hence, by focusing solar irradiation on this receiver, Heat Transfer Fluid (HTF) temperature increases [9]. Since this system is rather smaller and lighter than the conventional PTC, the receiver is fixed and parabolic trough reflector rotates to track the sun. Hence, a single-axis solar tracker is provided to adjust the reflector so that the absorber tube is at the focal point of the mirror throughout the day.

Table 1 shows the general characteristics of the PTC and Table 2 shows the material properties of the PTC.



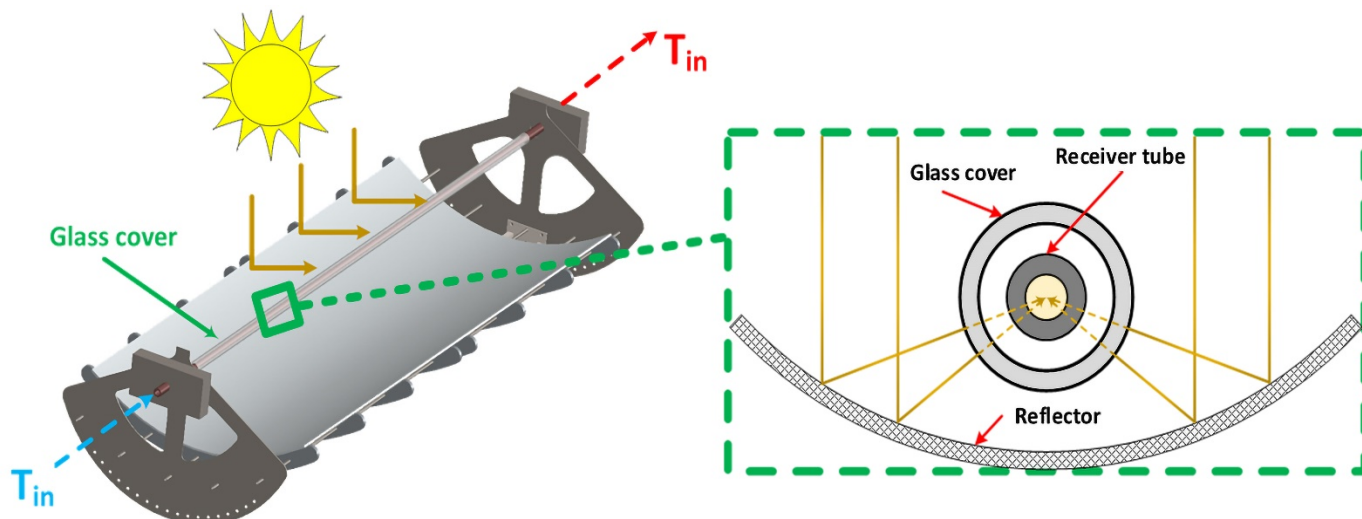


Figure 1. PTC experimental test facilities

Table 1. Characteristics of the PTC

Symbol	Parameter	Value	Unit
W	Width	1.2	m
L	Length	3	m
D_{ai}	Absorber inner diameter	25.4×10^{-3}	m
D_{ao}	Absorber outer diameter	28×10^{-3}	m
D_{gi}	Glass tube inner diameter	45×10^{-3}	m
D_{go}	Glass tube outer diameter	50×10^{-3}	m
F	Focal length	0.45	m
M	Weight	84.728	kg
T_{sun}	Sun's temperature	5780	K
ρ_{ref}	Collector reflectance	0.9	-
γ	Intercept factor	0.99	-
ϵ_r	Receiver emittance	0.23	-
ϵ_c	Cover emittance	0.9	-
σ	Stefan Boltzmann constant	5.6704×10^{-8}	W/m^2K^4
T	Cover transmittance	0.95	-
α	Absorber absorbance	0.967	-
V	Volumetric flow rate	50	L/min
K_r	Receiver thermal conductivity	401	W/mK
K_c	Cover thermal conductivity	1.14	W/mK
\dot{m}	Mass flow rate	0.06717	kg/s

Table 2. PTC's material properties

Parameter	Type
HTF	Shell Therimia B-S2
Collector	LS-2
Receiver tube	Copper
Cover material	Pyrex glass

Thermal oil (with brand Shell Therimia B) flows through the absorber tube as HTF with high heat transfer conductivity, excellent oxidation resistance, and resistance to a temperature range of 10 to 330 °C. Table 3 represents the technical specifications of this HTF at different temperatures.

Table 3. Technical specifications–Shell Therimia Oil B

Temperature	°C	0	20	40	100	150	200	250	300	340
Density	kg/m ³	876	863	850	811	778	746	713	681	655
Specific heat	J/kgK	1809	1882	1954	2173	2355	2538	2720	2902	3048
Thermal conductivity	W/mK	0.136	0.134	0.133	0.128	0.125	0.121	0.118	0.114	0.111
Prandtl	-	3375	919	375	69	32	20	14	11	9
Dynamic viscosity	kgm/s	0.2537	0.0654	0.0255	0.0041	0.0017	0.0010	0.0006	0.0004	0.0003

2.2. Data acquisition system

Data acquisition systems are one of the essential parts of empirical research. Accuracy of measurement, data verification, and control of conditions during the experiment are essential issues in data acquisition. This study measured inlet, outlet and ambient temperatures, HTF flow rate, wind

speed, and solar radiation intensity. The schematic of the test loop and instrument location and measurement device is shown in Figure 2. Furthermore, Table 4 demonstrates the characteristics of instruments such as type and accuracy as well as the specification of data acquisition system.

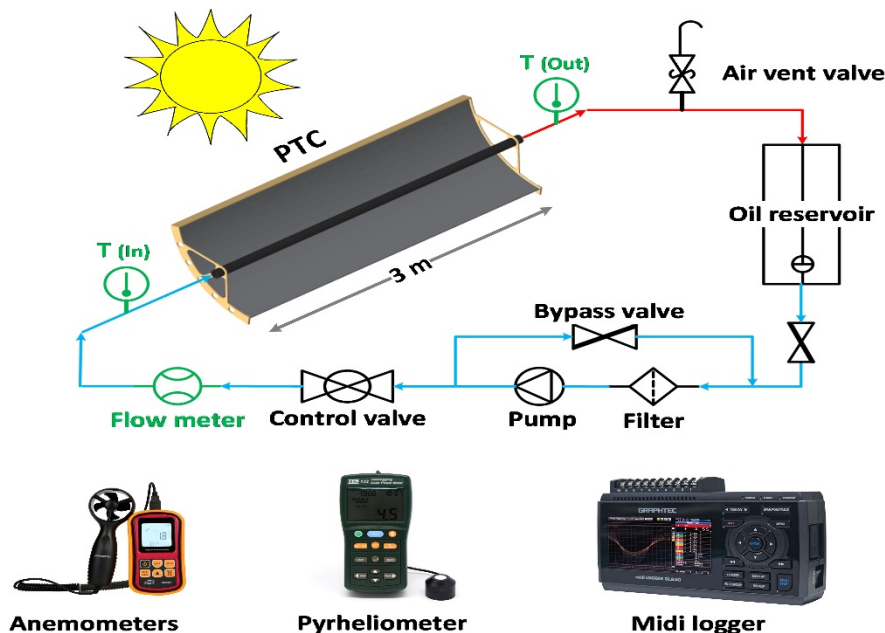


Figure 2. Schematic of the measurement system

Table 4. Characteristics of measuring instruments

Measuring instrument	Measurement parameter	Type	Range	Uncertainties
Midi-logger	Data acquisition-20 channel	Midi-840	Temperature, voltage, Ampere, Humidity	up to 10 Hz
Thermometer	Temperature	K-Type	(-40) – 1200 K	±0.5 °K
Flowmeter	Fluid flow rate	Rota Meter	0 – 5 L/min	±0.1 L/min
Pyrheliometer	Direct normal irradiation	TES 132	0 – 2000 W/m ²	±0.1 W/m ²
Anemometer	Wind velocity	GM89901	0 – 45 m/s	±0.1 m/s

3. MODELING AND SIMULATION

Based on the experimental facilities and experimental design tests, this study presented a precise analytical model using MATLAB software to compare not only the analytical model with experimental results but also predict further conditions applying different input dates on PTC. Based on the environmental conditions, physical and geometrical parameters of the PTC, the fluid outlet temperature, Glass cover temperature, receiver tube temperature, optical efficiency, and thermal efficiency are obtained. Figure 3 depicts the flowchart of the modeling and simulation procedure. As was mentioned earlier, in order to validate the analytical model first, the experimental investigation was conducted and implemented in the Matlab code. The results of the validation are represented in the next section. Another essential aim of analytical modeling is to extract further result data, which is very time-consuming and costly with the experimental investigation approach. In the following, hence, the influence of fluid temperature parameter, HTF type, and its flow rate on PTC thermal efficiency is also objective of analytical modeling.

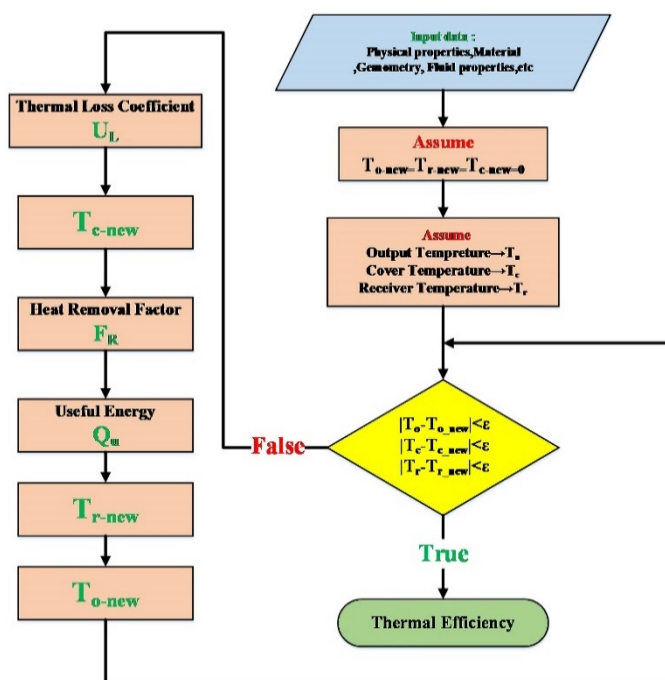


Figure 3. Modeling and simulation algorithm flow diagram

3.1. The governing equations

To obtain the part of solar radiation energy absorbed via the collector receiver and the heat dissipated to the environment, precise governing equations are implemented [21]. Thereby, using this data, the accurate thermal efficiency of the solar collector is achieved. Figure 4a demonstrates a schematic of the heat transfer model in the receiver of the PTC system. Furthermore, the detail of the thermal resistances network of the component from the HTF core to the environment is shown in Figure 4b.

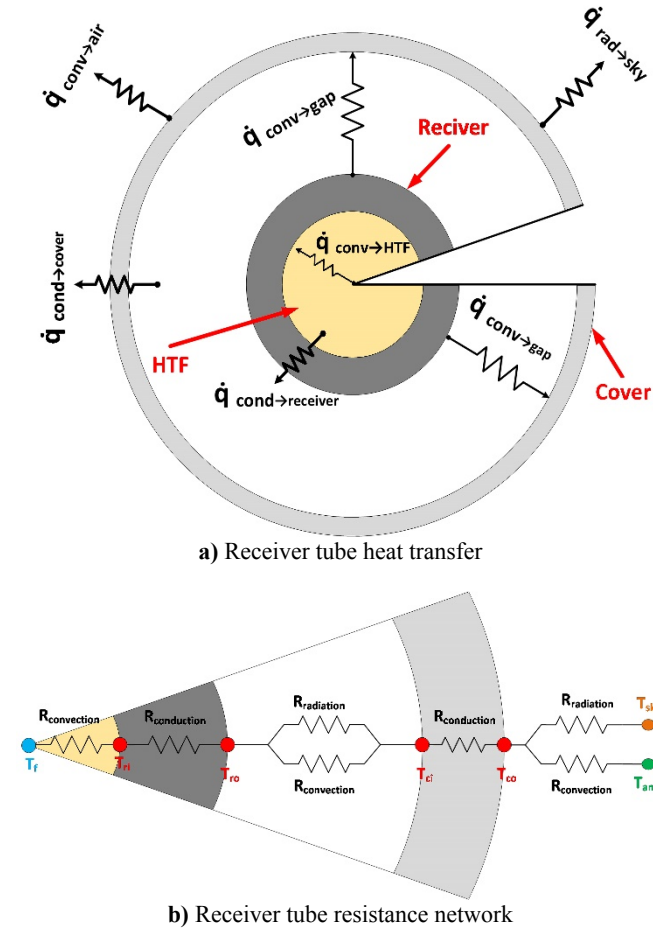


Figure 4. 2D heat transfer modeling of receiver tube

To measure the useful heat transferred, appropriate relationships for the collector efficiency factor F' , heat loss factor U_L , and the heat removal factor F_R must be derived. The heat removal coefficient in PTC, F_R , is calculated in the following [9].

$$F_R = \frac{M_f \times C_{p_f}}{A_r \times U_L} \left[1 - \exp\left(\frac{-A_r \times U_L \times F'}{M_f \times C_{p_f}}\right) \right] \quad (1)$$

A_r is the absorber area (m^2) and F' is the efficiency factor obtained using Eq. 2 [22].

$$F' = \frac{\frac{1}{U_L}}{\left(\frac{1}{U_L} + \frac{D_{ro}}{h_{cf} \times D_{ri}} + D_{ro} \times \frac{\ln\left(\frac{D_{ro}}{D_{ri}}\right)}{2 \times K_r} \right)} \quad (2)$$

where D_{ri} and D_{ro} are the inner and outer diameters of the absorber tube, respectively, and h_{cf} is the heat transfer

coefficient. The U_L , known as heat loss factor, can be calculated for two types of receivers: when the space between the absorber tube and the glass cover is vacuumed, U_L is calculated from Eq. 3; and when there is gas in this gap, U_L is calculated using Eq. 4 [9, 23].

$$U_L = \frac{1}{h_{r,r \rightarrow c} + \frac{A_r}{A_c} \times (h_{c,c \rightarrow am} + h_{r,c \rightarrow am})} \quad (3)$$

$$U_L = \frac{1}{h_{r,r \rightarrow c} + \frac{2 \times k_{gas,eff}}{D_{ci} \times \ln\left(\frac{D_{ci}}{D_{co}}\right)} + \frac{A_r}{A_c} \times (h_{c,c \rightarrow am} + h_{r,c \rightarrow am})} \quad (4)$$

Here, A_c is the cover area, A_r is the area of absorber tube, $h_{c,c \rightarrow am}$ is the heat transfer coefficient between glass cover and environment, $h_{r,c \rightarrow am}$ is the radiative heat transfer coefficient between cover and environment, $h_{r,r \rightarrow c}$ is the radiant heat transfer coefficient between the adsorbent and the cover, and $k_{gas,eff}$ is the effective heat transfer coefficient between the adsorbent and the glass cover.

Note, the heat transfer coefficient of displacement between the cover and the environment, $h_{c,c \rightarrow am}$, is obtained as follow:

$$h_{c,c \rightarrow am} = \frac{Nu_{air} \times K_{air}}{D_{co}} \quad (5)$$

where Nu_{air} is Nusselt number of air, which is calculated through the following equation [24].

$$Nu_{air} = C \times Re_{air}^M \times Pr_{air}^N \times \left(\frac{Pr_{air}}{Pr_W}\right)^{0.25} \quad (6)$$

The Prandtl number Pr_W was calculated at the outer surface temperature of the cover, and the other parameters of Relation 5 can be computed at the average temperature of the boundary layer between the cover and the air. The values of M, N, C are obtained from Table 5 [24].

Table 5. Constant for Eq. 6

Re	C	M	N	
			Pr < 10	Pr > 10
1 – 40	0.75	0.4	0.37	0.36
40 – 1000	0.51	0.5		
1000 – 2×10^5	0.26	0.6	0.37	0.36
2×10^5 – 10^7	0.076	0.7		

The radiative heat transfer coefficient between the cover and the environment $h_{r,c \rightarrow am}$ is obtained from the following relation.

$$h_{r,c \rightarrow am} = \epsilon_c \times \sigma \times (T_c^2 + T_{sky}^2) \times (T_c + T_{sky}) \quad (7)$$

where σ is Stephen Boltzmann's constant ($5.67 \times 10^{-8} \frac{W}{m^2 \times K^4}$), T_{sky} denotes the sky temperature, and T_c relates to the cover surface temperature with or without vacuum, which can be calculated through Relations 8 [25] and 9 [26], respectively.

$$T_{sky} = 0.05532 \times T_{amb}^{1.5} \quad (8)$$

$$T_{vac} = \frac{A_r h_{r,r \rightarrow c} \times T_r + A_c (h_{r,c \rightarrow am} + h_{c,c \rightarrow am}) T_{amb}}{A_r h_{r,r \rightarrow c} + A_c (h_{r,c \rightarrow am} + h_{c,c \rightarrow am})} \quad (9)$$

$$T_{cno-vac} = \frac{A_r h_{r,r \rightarrow c} + \left(\frac{2 \times k_{gas,eff}}{D_{ci} \times \ln\left(\frac{D_{ci}}{D_{co}}\right)} T_r\right) + A_c (h_{r,c \rightarrow am} + h_{c,c \rightarrow am}) T_{amb}}{A_r h_{r,r \rightarrow c} + \frac{2 \times k_{gas,eff}}{D_{ci} \times \ln\left(\frac{D_{ci}}{D_{co}}\right)} + A_c (h_{r,c \rightarrow am} + h_{c,c \rightarrow am})}$$

The value of the radiant heat transfer coefficient between the absorber tube and the cover $h_{r,r \rightarrow c}$ is obtained from Equation 10 as follows:

$$h_{r,r \rightarrow c} = \frac{\sigma \times (T_r^2 + T_c^2) \times (T_r + T_c)}{\frac{1}{\epsilon_r} + \left(\left(\frac{1}{\epsilon_c} - 1\right) \times \left(\frac{A_r}{A_c}\right)\right)} \quad (10)$$

where T_r represents the surface temperature of the adsorbent tube which can be calculated using Equation 11 [26].

$$T_r = T_{in} + \frac{Q_u}{A_r \times U_L \times F_R} \times (1 - F_R) \quad (11)$$

where Q_u is the useful heat transferred to the HTF. The effective heat transfer coefficient between the absorber tube and its cover, k_{gas_eff} , is as follows [23]:

$$k_{gas_eff} = 0.386 \times k \times \left(\frac{Pr_{r \rightarrow c}}{0.861 + Pr_{r \rightarrow c}}\right)^{0.25} \times Ra_{cy}^{0.25} \quad (12)$$

where k_{gas} is the conductivity heat transfer coefficient of the fluid between the absorber tube and the cover, and the Prandtl number $Pr_{r \rightarrow c}$ is obtained by considering the average temperature of the gas.

Further, the value of Ra_{cy} is obtained from Eq. 13 [23].

$$Ra_{cy} = \frac{\ln\left(\frac{D_{ci}}{D_{ro}}\right)^4 \times Ra}{L_c^3 \times (D_{ci}^{-0.6} + D_{ro}^{-0.6})^5} \quad (13)$$

where L_c represents the effective length and Ra represents the Riley dimensionless number. The last parameter needed to calculate the F_R is the heat transfer coefficient of the fluid h_{cf} and it can be obtained from the following relation [27].

$$h_{cf} = \frac{Nu_f \times K_f}{D_{ri}} \quad (14)$$

The value of Nu_f can also be calculated from Eq. 15 [28].

$$Nu_f = 3.66 + \frac{0.0667 \times Re_f \times Pr_f \times D_{ri}}{L \times \left(1 + 0.04 \times \left(\frac{Re_f \times Pr_f \times D_{ri}}{L}\right)^{\frac{2}{3}}\right)} \quad (15)$$

$$Nu_f = 0.023 \times Re^{0.8} \times Pr^{0.4}$$

$$Re < 2300$$

In Equation 15, parameter L represents the collector tube length and Pr_f is the Prandtl number of the fluid in the tube. In consequence, after calculating the heat removal factor, F_R , the useful heat transferred to the HTF can be obtained in the following [29]:

$$Q_u = F_R [(G \times \eta_{opt} \times A_a) - (A_r U_L (T_i - T_{amb}))] \quad (16)$$

where the parameter G is the solar radiation intensity, A_a is area, and η_{opt} is the optical efficiency of the collector. Assuming that the solar radiation is perpendicular to the reflector span at any moment, the optical efficiency can be computed as follows:

$$\eta_{opt} = \rho_{ref} \times \tau \times \alpha \times Y \quad (17)$$

where α , τ , Y and ρ_{ref} are the absorption coefficient, the cover transmittance, the intercept factor, and the collector reflectance, respectively. Meanwhile, the thermal efficiency is obtained from Equation 18 [9].

$$\eta_{th} = \frac{Q_u}{G \times A_a} \times 100 \quad (18)$$

where Q_u is the transferred useful heat to the HTF. Consequently, the HTF temperature difference is obtained from Eq. 18 below:

$$\Delta T = \left(\frac{A_a \times \eta_{th}}{\dot{m} \times c_p}\right) \times G \quad (19)$$

3.2. Validation

To show the robustness of the simulation, the validation process is a mandatory step. For this purpose, the obtained results from the experimental investigation should be compared with the analytical simulation. The experimental results obtained for a wide range of inlet temperatures and velocities are presented in Table 6. The fluid output temperature of the collector and its thermal efficiency in the experimental and numerical modeling are compared to confirm the accuracy of the modeling performance.

Table 6. Comparison between experimental result and numerical model

HTF flow rate = 0.06717 kg/s										
Date	G_b (W/m ²)	T_{amb} (°C)	T_{in} (°C)	V_{wind} (m/s)	T_{out} (°C)			η_{th} (%)		
					EXP	Model	Error (%)	EXP	Model	Error (%)
2018/10/21	667	21.6	47.80	1.7	59.86	60.39	0.89	70.55	73.69	4.45
2018/10/21	676	22.9	54.50	2	66.81	67.03	0.33	71.91	73.21	1.82
2018/10/21	685	24.5	45.39	1.4	58.10	58.43	0.56	72.17	74.04	2.60
2018/10/21	767	25.5	42.73	0.9	58.29	57.43	1.47	76.67	74.29	-5.58
2018/10/21	882	25.6	46.62	1.4	62.99	63.23	0.39	72.56	73.67	1.53
2018/10/22	450	23.7	54.35	0.7	62.81	62.78	0.05	74.01	73.73	-0.37
2018/10/22	557	24.3	50.79	2.2	60.84	61.25	0.66	70.69	73.56	4.06
2018/10/22	414	24.15	44.88	0.5	53.09	52.87	0.41	76.72	74.67	-2.67
2018/10/22	587	24.15	45.74	2.3	56.89	56.91	0.03	73.77	73.89	0.16
2018/10/22	617	24.5	38.29	1.9	50.11	50.27	0.32	73.48	74.47	1.35
2018/10/23	613	17.5	39.84	0.9	51.65	51.70	0.09	74.08	74.39	0.42
2018/10/23	674	21.75	52.10	1.3	64.93	64.70	0.36	74.93	73.54	-1.85
2018/10/23	663	24.05	47.07	0.8	59.36	59.68	0.54	72.28	74.18	2.63
2018/10/23	715	24.45	48.59	1.2	62.42	62.08	0.54	75.71	73.86	-2.45

2018/10/23	874	23.75	49.10	1.6	65.79	65.44	0.53	75.02	73.43	-2.12
2018/10/24	758	22.70	39.67	1.9	53.95	54.23	0.52	72.63	74.06	1.97
2018/10/24	717	23.00	48.79	1.5	62.10	62.28	0.30	72.67	73.69	1.41
2018/10/24	790	24.55	49.02	0.5	64.51	63.94	0.88	76.92	74.07	-3.71
2018/10/24	852	25.20	50.36	1	66.73	66.31	0.63	75.62	73.65	-2.60
2018/10/24	888	24.90	47.75	0.8	64.68	64.47	0.32	74.75	73.81	-1.26

According to the results of Table 6, the maximum error associated with the fluid outlet temperature in analytical modeling is 1.47 % and the maximum error of thermal efficiency is 5.58. The analytical and experimental results are compared in Figures 5 and 6 the error interval in each case is determined.

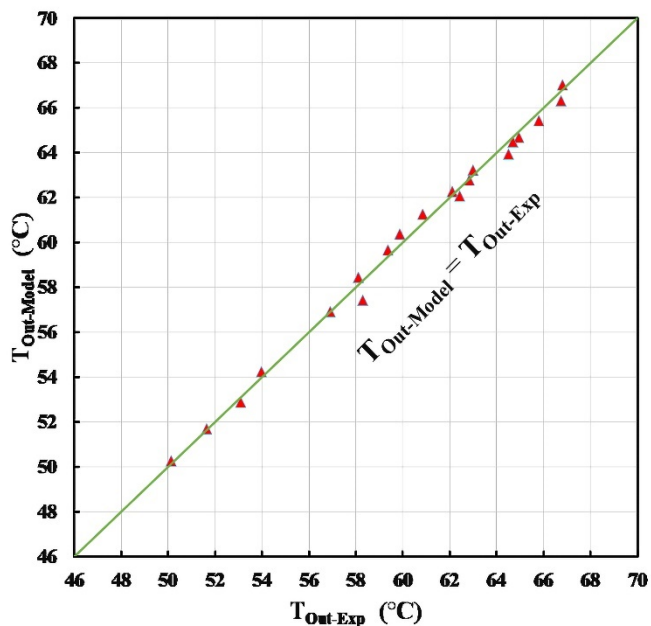


Figure 5. Comparison of the outlet temperature in analytical and experimental results

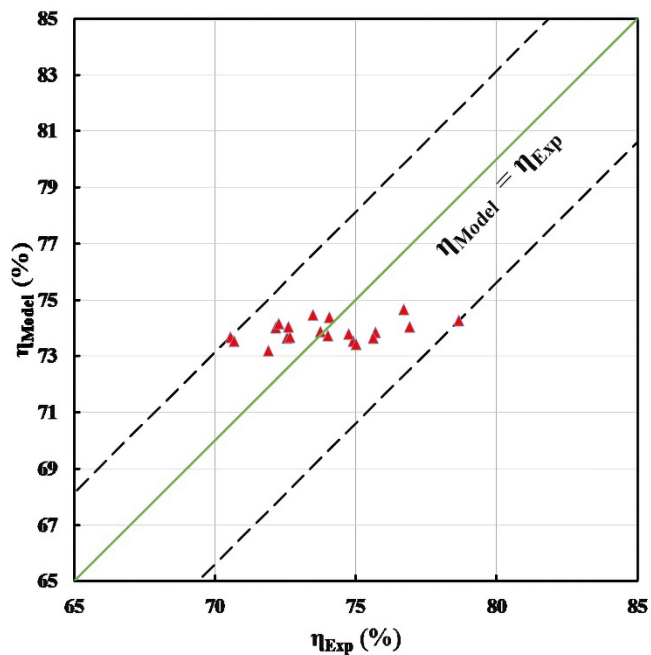


Figure 6. Comparison of the efficiency in analytical and experimental results

Accordingly, the right consistency is obtained between analytical and experimental results. Moreover, to make a better comparison between the experimental and analytical data, Figure 7 shows the temperature difference between inlet and outlet temperatures against solar radiation in both analytical and experimental cases.

The linear trend equation for both analytical and experimental investigations is demonstrated in this figure. Upon comparing the slope values of the experimental and analytical data in Figure 7, there is only 0.53 % error which shows the good accuracy of the analytical modeling approach.

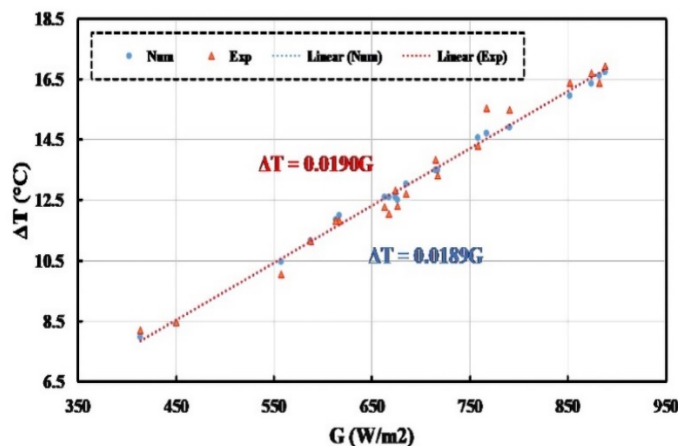


Figure 7. Comparison of HTF temperature difference between experimental and analytical results

4. RESULTS AND DISCUSSION

4.1. Mass Flow Rate Effect

The operating conditions of PTC influence thermal efficiency. Solar radiation, wind speed, and ambient temperature are the major affected factors. Calculation is carried out at a specified time interval, presuming that the wind speed and ambient temperature are constant. Figure 8 depicts the difference between the inlet and outlet HTF temperatures (ΔT) versus solar irradiation. According to Eq. 19, since ΔT is a function of PTC efficiency and HTF specific heat capacity, the slope of the fluid temperature diagram is fairly constant. Therefore, linear behavior for any HTF flow rate can be expected. In Figure 8, 8 different discharge flow rates are plotted.

According to Figure 8, as the HTF flow rate increased with the same solar irradiation ranges, the slope of the graph and, hence, the HTF temperature difference decrease. Furthermore, according to Figure 8, at specific solar irradiation, ΔT of HTF is more influential in the HTF flow rate. In other words, if more ΔT is targeted, the decrease of HTF flow rate is appreciated. For more clarity, Table 7 demonstrates the HTF mass flow rate with respect to the slope of the graphs in Figure 8. According to Eq. 19, the line slope is $(\frac{A_a \times \eta_{th}}{m \times C_p})$, called capacity factor.

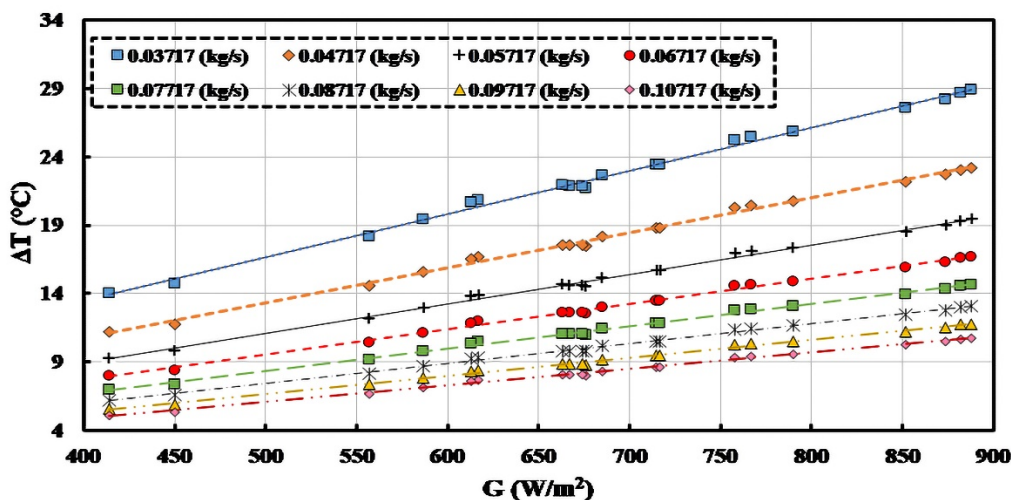


Figure 8. Effect of mass flow rate on the temperature difference for S2

Table 7. Capacity factor values for different mass flow rates

#	Mass flow rate (kg/s)	$\frac{A_a \times \eta_{th}}{\dot{m} \times C_p}$
1	0.03717	0.0328
2	0.04717	0.0263
3	0.05717	0.0220
4	0.06717	0.0189
5	0.07717	0.0166
6	0.08717	0.0148
7	0.09717	0.0133
8	0.10717	0.0121

slope is in fact related to PTC thermal efficiency and HTF heat capacity ($\frac{\eta_{th}}{C_p}$).

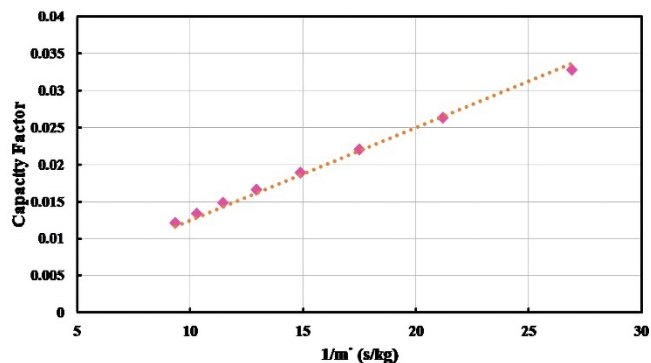
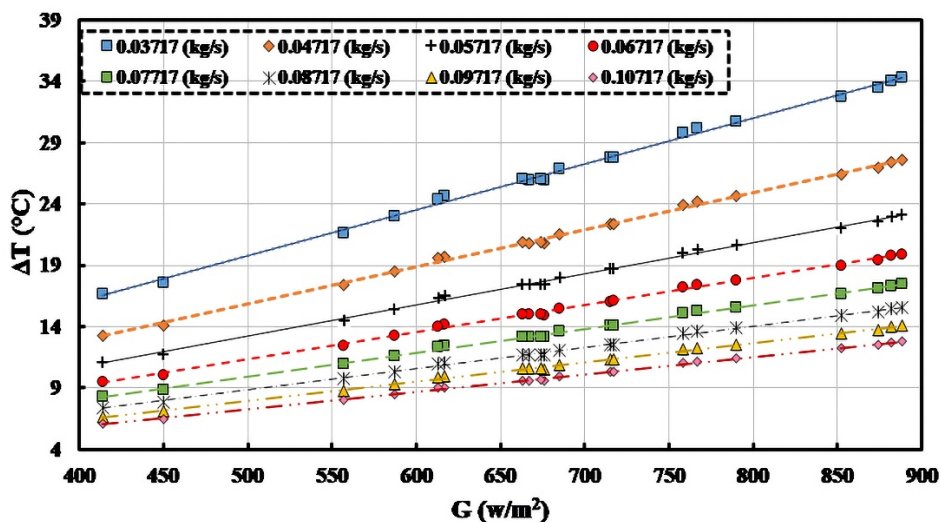


Figure 9. Variation in capacity factor against the inverse of mass flow rate

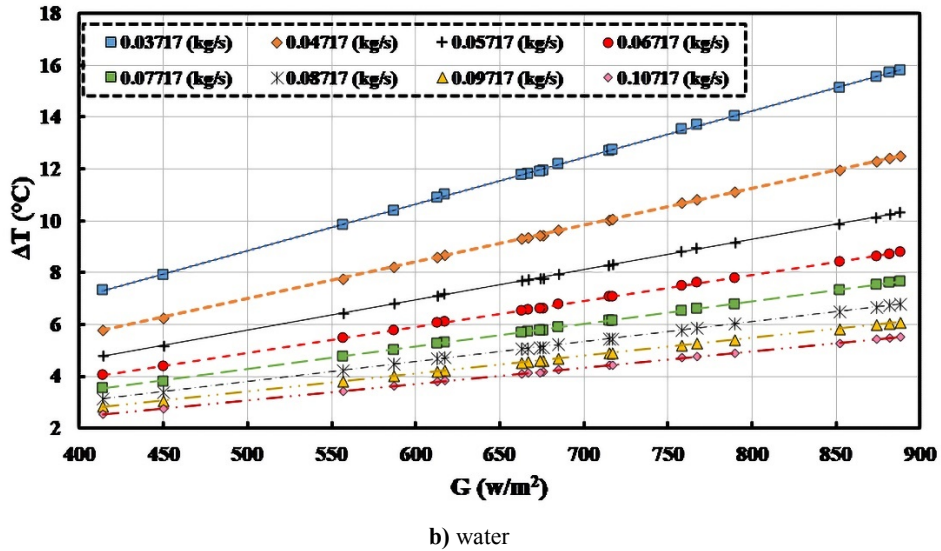
According to the data illustrated in Table 7, the increase of mass flow rate is consistent with the decreasing of the capacity factor values. Furthermore, according to Eq. 19, the slope of the linear trends in Figure 8 corresponds with the inverse of mass flow rate ($\frac{1}{\dot{m}}$). Therefore, for clarity, if capacity factor is plotted against the reverse of mass flow rate, Figure 9 is formed. According to Figure 9, an excellent linear approximation can be obtained. It is inferred that the line

4.2. Influence of HTF type

To examine the influence of HTF type, a similar investigation is performed for two other fluids: Syltherm 800 and water. The results are obtained and illustrated in Figure 10. The HTF temperature difference at different solar irradiation and mass flow rates is depicted in this figure for two HTF types.



a) Syltherm 800



b) water
Figure 10. Effect of mass flow rate on the temperature difference

Figure 10 reveals that in the same condition, the HTF temperature difference in Syltherm 800 oil is higher than water, which can be attributed to its lower thermal capacity than water. Meanwhile, the reduction of the capacity factor due to an increase in the HTF flow rate is shown for the three HTF types of S2 oil, Syltherm 800 oil, and water (Figure 11) to better elucidate the effect of the HTF types. According to Figure 12, the term capacity factor for the Syltherm 800 oil is more responsive to the reduction of the HTF flow rate (increasing 1/m) compared to S2 and water. It is shown that to reach a higher temperature at a constant flow rate and solar irradiation, Syltherm 800 oil is better than S2 oil and S2 oil is better than water.

and 8.33 %, respectively, but it is negligible for the water. It can be attributed to the higher heat capacity of the water than other HTFs considered in this study. The high heat capacity of water causes a decrease in the absorber surface temperature, which has a high impact on the receiver heat loss. This outstanding result is discussed in the following.

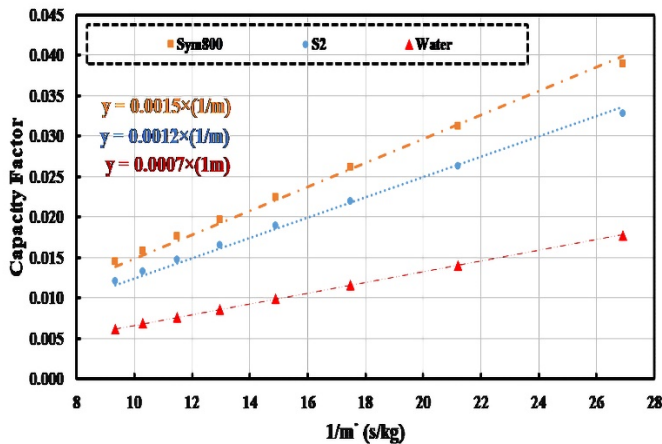


Figure 11. Variation in capacity factor against the inverse of mass flow rate for three different HTFs

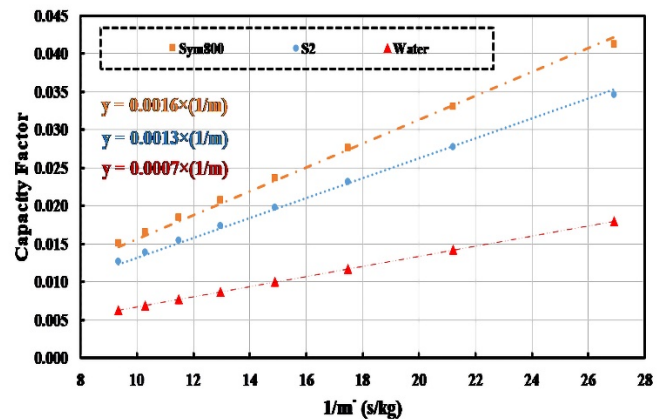


Figure 12. Effect of the vacuum on the variation of capacity factor with respect to the inverse of mass flow rate for three different HTF types

4.3. The effect of vacuum

The effect of the vacuum in the gap between the glass cover and the absorber tube on the thermal performance is investigated. Thereby, the governing equations of the solar vacuum tube are implemented in the analytical model for different HTFs to obtain thermal factors. The results are depicted in Figure 12 for three HTF. As expected, implementing a vacuum tube will enhance the capacity factor more than the non-vacuumed tube (see Figure 11). This graph shows that the rates of the effectiveness of the evacuated tube in capacity factor for Syltherm 800 oil and S2 oil are 6.66 %,

4.4. Temperature distribution of PTC

Furthermore, in the PTC system, another factor affecting the heat transfer rate and outlet HTF temperatures is the surrounding conditions of PTC such as the intensity of solar radiation, wind speed, and ambient and sky temperatures. These factors influence the temperature of various points of the receiver of PTC, such as the glass cover temperature as well as the surface temperature of the absorber tube, which affect the rate of heat transfer to the HTF. According to the model illustrated in Figure 5, the temperature distribution of the receiver can elucidate the heat transfer mechanism. In a specific surrounding condition listed in Table 8, use of 2D numerical model and simulation in the radial direction of the receiver is considered for three different HTF types for the receiver with & without vacuum. Accordingly, the temperature distribution in the radial direction is obtained and plotted in Figure 13 for three HTFs of Syltherm 800 oil, S2 oil and water.

Table 8. Governing condition of Figure 13

Flow rate (kg/s)	Ambient temperature (°C)	Wind speed (m/s)	Solar irradiance (W/m ²)	HTF inlet temperature (°C)
0.067 17	21.6	1.7	667	47.8

As can be seen in Figure 13, the highest temperature for the receiver in the PTC is the outer surface temperature of the absorber tube and the lowest temperature is the outer surface temperature of the glass cover. The smallest temperature difference between the absorber tube and the HTF occurs for the water, and the biggest one is in Syltherm 800 oil, which is owing to the HTF thermo-physical properties, especially the specific heat capacity. Furthermore, the impact of the vacuum on the temperature is demonstrated in Figure 13. As can be

seen, the overall temperature in the vacuomed tube is higher than that in the unvacuomed tube. However, the level of temperature for the vacuomed tube is higher for the Sym800 and S2 than that for the water.

4.5. Thermal efficiency effect

In consequence, this study calculated the thermal efficiency of the PTC for three different HTFs, flow rate ranging from 0.0372 to 0.1072 kg/s, and solar radiation from 400 to 900 W/m².

To obtain the thermal efficiency, the environmental conditions demonstrated in Table 8 are applied for 8 different HTF flow rates and wide ranges of solar irradianations. The results are depicted in Figure 14 for three HTFs used in this study.

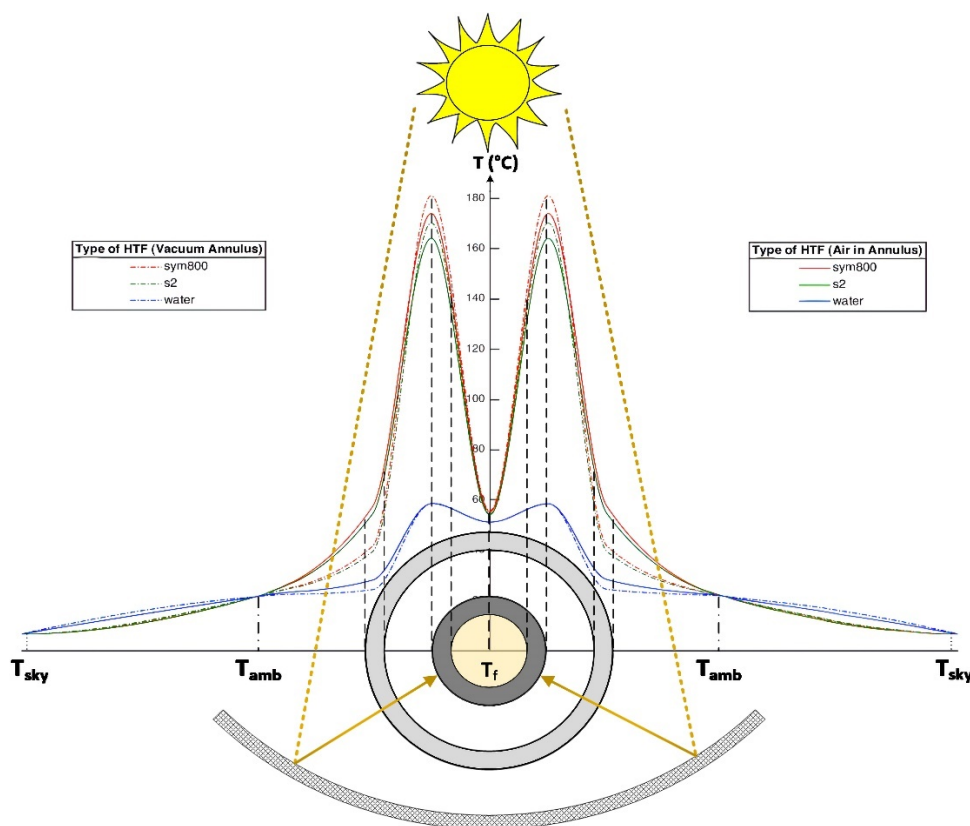
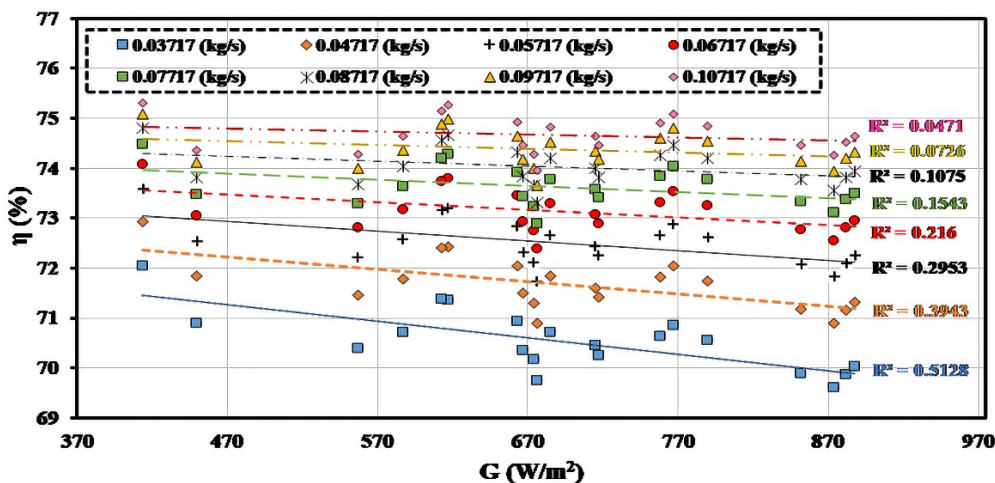


Figure 13. Temperature profile of PTC for vacuomed & unvacuomed tubes and three HTF types



a) Syltherm 800

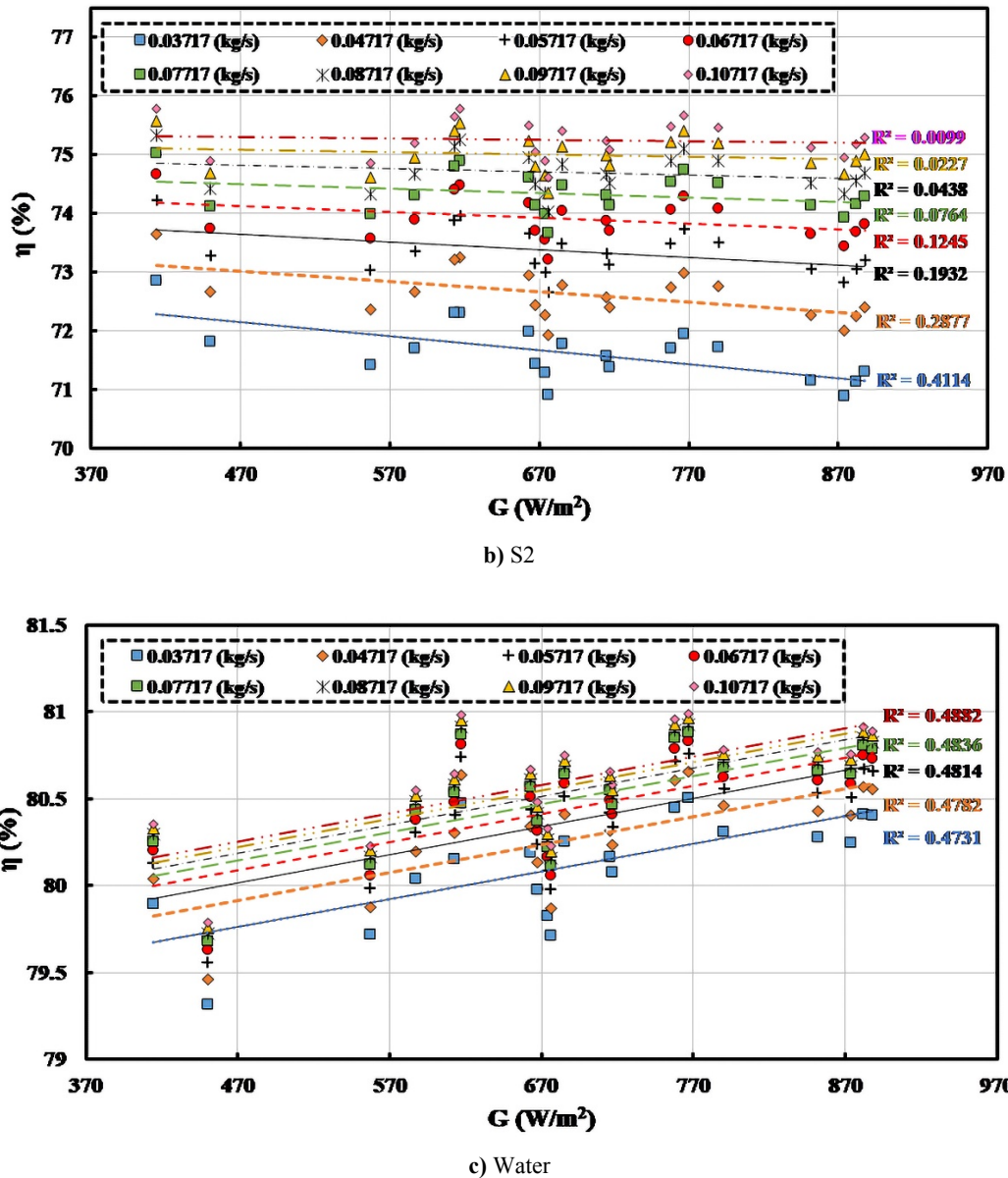
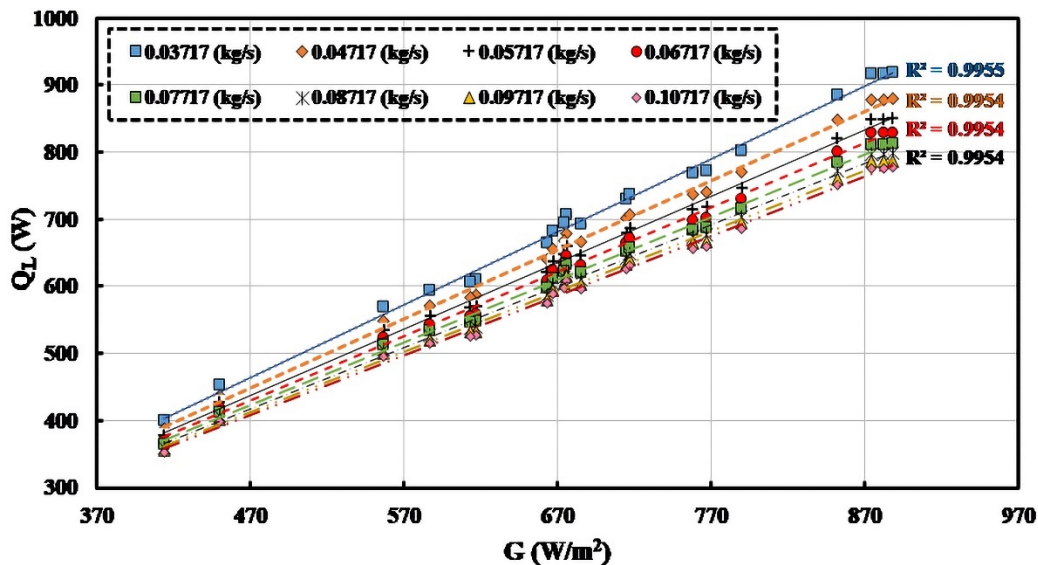


Figure 14. Effect of mass flow rate and solar irradiation on thermal efficiency for three HTF types

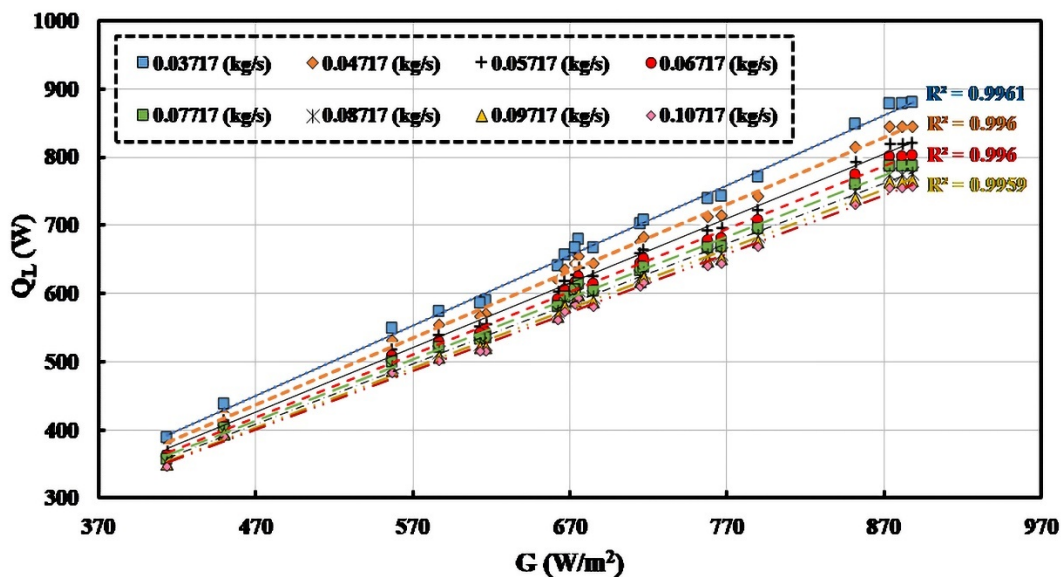
According to Figure 14, the thermal efficiency raises with an increase in the HTF flow rate and decreases following the growth of solar radiation for Syltherm 800 and S2. The opposite behavior is seen for water, which is explicitly discussed in the paragraph below. Further, with the increment of the HTF flow rate, the Reynold number increases in the absorber tube. Therefore, it leads to an increase in the heat transfer coefficient, which consequently results in thermal efficiency rise at a higher HTF flow rate. Moreover, according to Figure 14, the thermal efficiencies obtained for the lower HTF are more scattered around the fitted line than the higher flow rate. The R-square is given in Figure 14 for all trend lines. It can be confirmed that the model is excellent consistent with the high flow rate.

The behavior of decrement of thermal efficiency with the solar radiation for Syltherm 800 and S2 is attributed to the heat loss from the receiver to the environment due to the hot surface of the receiver at higher solar irradiation. According to Figure 15c, the behavior of water differs from the other two

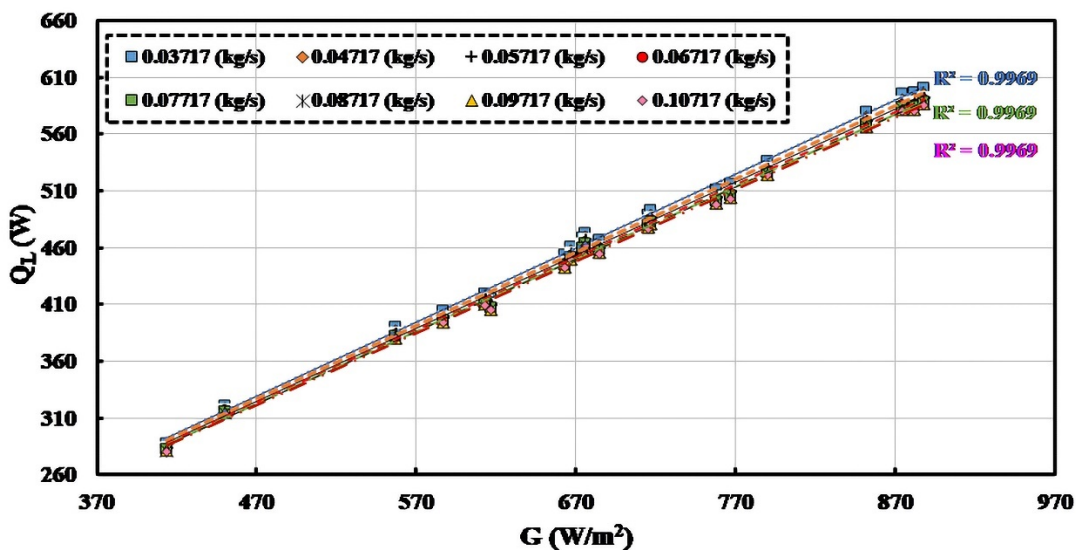
HTFs. To assess this behavior, heat loss is calculated based on the analytical model shown in Figure 4 for three different HTFs. The results are depicted in Figure 15. Accordingly, the heat loss for Syltherm 800 and S2 is much higher than that for the water. It can be attributed to the high temperature of the absorber tube of Syltherm 800 and S2, compared to water. Compared to the two other HTFs, water with higher specific thermal heat and heat transfer conductivity would diminish absorber tube temperature. The impact of solar intensity variations on the temperature distribution across the horizontal cross-section of the PTC is shown in Figure 16 for the three HTFs. This figure confirms that the same value of solar intensity could produce maximum temperature on the absorber tube for Syltherm 800 as a working fluid compared to S2 and water as a working fluid. Therefore, based on the conditions examined in this study, it can be concluded that water can cool down the absorber to gain more solar heat than the two other HTFs. However, the HTF temperature is lower for the water.



a) Syltherm 800



b) S2



c) Water

Figure 15. Heat loss in three HTFs with different flow rates and solar irradiancies

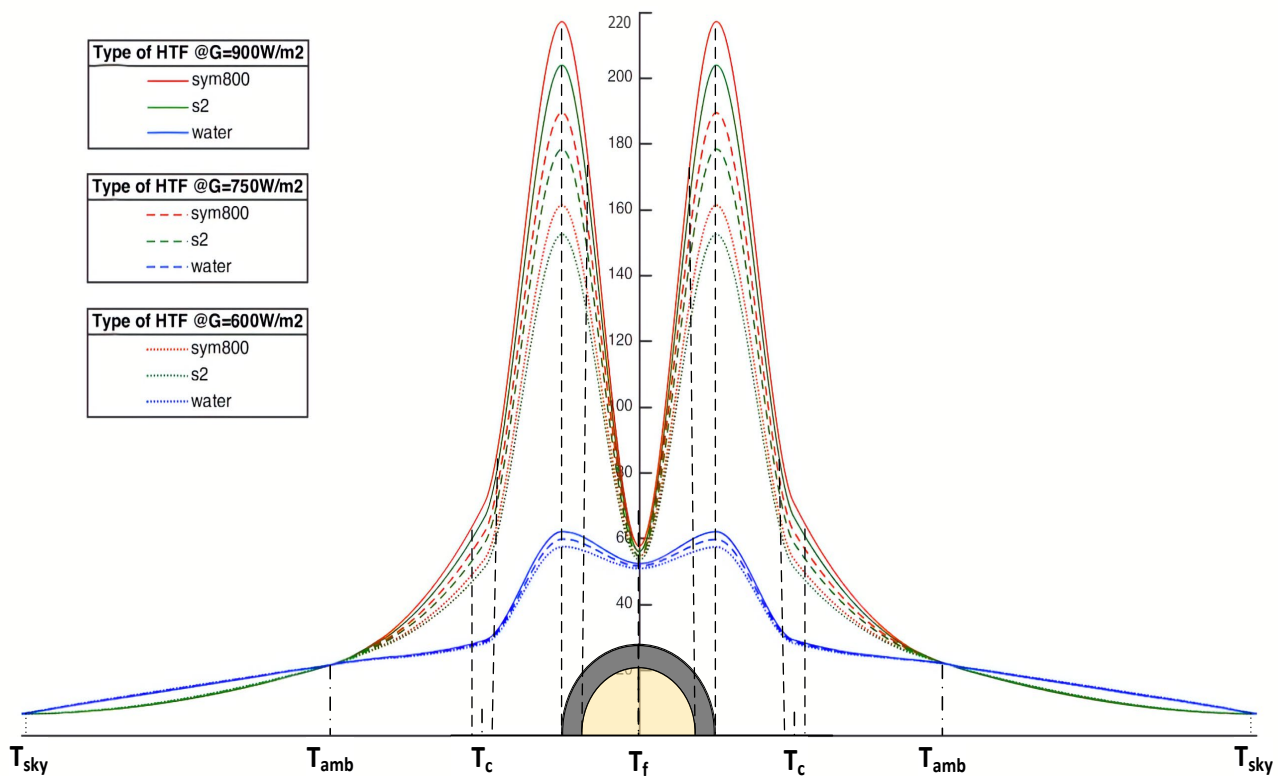


Figure 16. Temperature distribution for three HTFs and three irradiances

5. CONCLUSIONS

This study managed to carry out an experiment with the aim of investigating different rates of thermal efficiency, temperature distribution of a PTC for varying mass flow rates, and solar intensities for three Heat Transfer Fluid (HTF) types. In addition, the results were validated using a developed numerical model. In this regard, the PTC was employed and an experimental rig was built to perform the experimental study. Moreover, the effect of the vacuum in the space among the glass cover and the adsorbent tube was examined for these three HTFs. The following results can be concluded through this research:

- There was a linear relationship between the temperature change across the PTC and the variation of the HTF flow rate for constant solar radiation. The slope of these changes represents the sensitivity of these three HTFs. The results showed that the Syltherm 800 oil was more sensitive to the variation of the HTF flow rates than S2 oil and ordinary water. In other words, a higher temperature was available for a lower mass flow rate with a PTC and Syltherm 800.

- The linear relationship between the capacity factor and the inverse of mass flow rate demonstrated that the PTC with Syltherm 800 had a greater degree of thermal efficiency than the other two HTFs with PTC.

- The results for the presence of the vacuum between the glass cover and the adsorbent tube indicated that the existence of vacuum raised the thermal efficiency of PTC with Syltherm 800 oil by about 6.7 %, about 8.3 % with S2 oil, and a negligible amount for ordinary water.

- The temperature profile across the horizontal cross-section of the PTC with three working fluids (constant solar intensity

and HTF mass flow rate) showed that maximum temperature was reached on the receiver tube and this maximum temperature for Syltherm 800 oil was 176 °C and for S2 oil and water were 161 °C and 61 °C, respectively.

- The presence of the vacuum between the glass cover and the adsorbent tube changed the maximum temperature of the receiver tube with Syltherm 800 oil by about 2.84 % from 176 °C to 181 °C, for S2 oil by about 3.72 % from 161 °C to 167 °C, and by negligible amount for water.

- The results for the effects of solar intensity variation on the temperature profile across the horizontal cross-section of the PTC with three working fluids revealed that the maximum temperature still occurs on the receiver tube. However, the maximum temperature of the receiver tube with Syltherm 800 oil working fluid increased by 35.1 % from 167 °C to 219 °C, since the solar intensity changed from 600 W/m² to 900 W/m². This increase in the case of the same level of solar intensity variation for S2 working fluid was 32.7 % from 153 °C to 203 °C. Again, this temperature rise for water as a working fluid was about 6.8 %, which is almost negligible in comparison with that for these two oils as working fluids.

In the end, it should be noted that despite the proof of the existing modeling, it is better to evaluate the results with experimental research in future research, for which special facilities and equipment are required that make these studies limited and difficult.

6. ACKNOWLEDGEMENT

The authors acknowledge the support of renewable energy systems laboratory of Iran University of Science and Technology.

NOMENCLATURE

A	Area (m ²)
C	Concentration
C _p	Specific heat at constant pressure (kJK ⁻¹ kg ⁻¹)
D	Diameter (m)
F	Focal distance (m)
F _R	Heat removal factor
h	Heat transfer coefficient (Wm ⁻² K)
G	Solar radiation (Wm ⁻²)
K	Thermal conductivity (WK ⁻¹ m ⁻¹)
Nu	Nusselt number
T	Temperature (C)
Pr	Prandtl number
Q _u	Useful energy (W)
Re	Reynolds number
U _L	Collector loss coefficient (Wm ⁻² K ⁻¹)
V _{air}	Air velocity (ms ⁻¹)
W	Width (m)
L	Tube length (m)
Ra	Rayleigh number

Greek letters

α	Absorber absorbance
ρ _{ref}	Collector reflectance
γ	Intercept factor
μ	Dynamic viscosity (kgm ⁻¹ s ⁻¹)
ε	Emissance
η	PTC efficiency
η _{opt}	Optical efficiency
ρ	Density (kgm ⁻³)
σ	Stefan-Boltzmann constant (Wm ⁻² K ⁻⁴)
τ	Cover transmittance

Subscripts

sky	Sky condition
f	Fluid inlet
out	Outlet
in	Inlet
opt	Optical
c	Cover
r	Receiver
a	Aperture
i	Inner
o	Outer
amb	Ambient
L	Loss

Abbreviation

CSP	Concentrating Solar Power
DNI	Direct Normal Irradiance
LS-2	Lus System 2 End Gen
SNL	Sandia National Laboratory
PTC	Parabolic Trough Collector
SNL	Sandia National Laboratory

REFERENCES

- Borzuei, D., Moosavian, S.F. and Farajollahi, M., "On the performance enhancement of the three-blade savonius wind turbine implementing opening valve", *Journal of Energy Resources Technology*, Vol. 143, No. 5, (2021). (<https://doi.org/10.1115/1.4049460>).
- Zahedi, R., Ahmadi, A. and Sadeh, M., "Investigation of the load management and environmental impact of the hybrid cogeneration of the wind power plant and fuel cell", *Energy Reports*, Vol. 7, (2021), 2930-2939. (<https://doi.org/10.1016/j.egy.2021.05.008>).
- Kizilkan, O., Kabul, A. and Dincer, I., "Development and performance assessment of a parabolic trough solar collector-based integrated system for an ice-cream factory", *Energy*, Vol. 100, (2016), 167-176. (<https://doi.org/10.1016/j.energy.2016.01.098>).
- Jamar, A., Majid, Z., Azmi, W., Norhafana, M. and Razak, A., "A review of water heating system for solar energy applications", *International Communications in Heat and Mass Transfer*, Vol. 76, (2016), 178-187. (<https://doi.org/10.1016/j.icheatmasstransfer.2016.05.028>).
- Chahine, K., Murr, R., Ramadan, M., Hage, H.E. and Khaled, M., "Use of parabolic troughs in HVAC applications—Design calculations and analysis", *Case Studies in Thermal Engineering*, Vol. 12, (2018), 285-291. (<https://doi.org/10.1016/j.csite.2018.04.016>).
- Ahmadi, A., Ehyaei, M.A., Doustgani, A., El Haj Assad, M., Hmida, A., Jamali, D.H., Kumar, R., Li, Z.X. and Razmjoo, A., "Recent residential applications of low-temperature solar collector", *Journal of Cleaner Production*, (2020), 123549. (<https://doi.org/10.1016/j.jclepro.2020.123549>).
- Marefati, M., Mehrpooya, M. and Shafii, M.B., "Optical and thermal analysis of a parabolic trough solar collector for production of thermal energy in different climates in Iran with comparison between the conventional nanofluids", *Journal of Cleaner Production*, Vol. 175, (2018), 294-313. (<https://doi.org/10.1016/j.jclepro.2017.12.080>).
- Abid, M., Ratlamwala, T. and Atikol, U., "Performance assessment of parabolic dish and parabolic trough solar thermal power plant using nanofluids and molten salts", *International Journal of Energy Research*, Vol. 40, No. 4, (2016), 550-563. (<http://doi.org/10.1002/er.3479>).
- Kalogirou, S.A., *Solar energy engineering: Processes and systems*, Academic Press, (2013). ([https://www.google.com/books/edition/Solar_Energy_Engineering/wYRqAAAAQBAJ?hl=en&gbpv=1&dq=Kalogirou,+S.A.,+Solar+energy+engineering:+Processes+and+systems,+Academic+Press,+2013\)&pg=PI&printsec=frontcover](https://www.google.com/books/edition/Solar_Energy_Engineering/wYRqAAAAQBAJ?hl=en&gbpv=1&dq=Kalogirou,+S.A.,+Solar+energy+engineering:+Processes+and+systems,+Academic+Press,+2013)&pg=PI&printsec=frontcover)).
- Ghodbane, M. and Boumeddane, B., "A numerical analysis of the energy behavior of a parabolic trough concentrator", *Journal of Fundamental and Applied Sciences*, Vol. 8, No. 3, (2016), 671-691. (<http://doi.org/10.4314/jfas.v8i3.2>).
- Yaghoubi, M., Ahmadi, F. and Bandehee, M., "Analysis of heat losses of absorber tubes of parabolic trough collector of Shiraz (Iran) solar power plant", *Journal of Clean Energy Technologies*, Vol. 1, No. 1, (2013), 33-37. (<http://10.7763/JOCET.2013.V1.8>).
- Ibrar Hussain, M., Mokheimer, E. and Ahmed, S., "Optimal design of a solar collector for required flux distribution on a tubular receiver", *Journal of Energy Resources Technology*, Vol. 139, No. 1, (2017). (<http://doi.org/10.1115/1.4035361>).
- Kalogirou, S.A., "Solar thermal collectors and applications", *Progress in Energy and Combustion Science*, Vol. 30, No. 3, (2004), 231-295. (<https://doi.org/10.1016/j.peccs.2004.02.001>).
- Bellos, E., Tzivanidis, C. and Tsimoukakis, D., "Multi-criteria evaluation of parabolic trough collector with internally finned absorbers", *Applied Energy*, Vol. 205, (2017), 540-561. (<https://doi.org/10.1016/j.apenergy.2017.07.141>).
- Bellos, E. and Tzivanidis, C., "Investigation of a star flow insert in a parabolic trough solar collector", *Applied Energy*, Vol. 224, (2018), 86-102. (<https://doi.org/10.1016/j.apenergy.2018.04.099>).
- Xiao, X., Zhang, P., Shao, D. and Li, M., "Experimental and numerical heat transfer analysis of a V-cavity absorber for linear parabolic trough solar collector", *Energy Conversion and Management*, Vol. 86, (2014), 49-59. (<https://doi.org/10.1016/j.enconman.2014.05.001>).
- Bellos, E. and Tzivanidis, C., "Thermal analysis of parabolic trough collector operating with mono and hybrid nanofluids", *Sustainable Energy Technologies and Assessments*, Vol. 26, (2018), 105-115. (<https://doi.org/10.1016/j.seta.2017.10.005>).
- Boukelia, T., Mecibah, M. and Laouafi, A., "Performance simulation of parabolic trough solar collector using two fluids (thermic oil and molten salt)", *Journal of Fundamental and Applied Sciences*, Vol. 8, No. 2, (2016), 600-626. (<https://doi.org/10.4314/jfas.v8i2.28>).
- Dudley, V.E., Kolb, G.J., Mahoney, A.R., Mancini, T.R., Matthews, C.W., Sloan, M. and Kearney, D., "Test results: SEGS LS-2 solar collector", Nasa STI/Recon Technical Report N, Vol. 96, (1994), 11437. (<https://doi.org/10.2172/70756>).
- Reddy, K., Kumar, K.R. and Ajay, C., "Experimental investigation of porous disc enhanced receiver for solar parabolic trough collector", *Renewable Energy*, Vol. 77, (2015), 308-319. (<https://doi.org/10.1016/j.renene.2014.12.016>).
- Chowdhury, M. and Mokheimer, E., "Recent developments in solar and low-temperature heat sources assisted power and cooling systems: A design perspective", *Journal of Energy Resources Technology*, Vol. 142, No. 4, (2020). (<https://doi.org/10.1115/1.4044562>).
- Moosavian, S.F., Borzuei, D. and Ahmadi, A., "Energy, exergy, environmental and economic analysis of the parabolic solar collector with life cycle assessment for different climate conditions", *Renewable Energy*, Vol. 165, (2021), 301-320. (<https://doi.org/10.1016/j.renene.2020.11.036>).
- Behar, O., Khellaf, A. and Mohammedi, K., "A novel parabolic trough solar collector model—Validation with experimental data and comparison to Engineering Equation Solver (EES)", *Energy Conversion*

- and Management*, Vol. 106, (2015), 268-281. (<https://doi.org/10.1016/j.enconman.2015.09.045>).
24. Tagle-Salazar, P.D., Nigam, K. and Rivera-Solorio, C.I., "Heat transfer model for thermal performance analysis of parabolic trough solar collectors using nanofluids", *Renewable Energy*, Vol. 125, (2018), 334-343. (<http://10.1016/j.renene.2018.02.069>).
25. Swinbank, W.C., "Long-wave radiation from clear skies", *Quarterly Journal of the Royal Meteorological Society*, Vol. 89, No. 381, (1963), 339-348. (<https://doi.org/10.1002/qj.49708938105>).
26. Duffie, J.A. and Beckman, W.A., *Solar engineering of thermal processes*, John Wiley & Sons, (2013). (<https://doi.org/10.1002/9781118671603>).
27. Tzivanidis, C. and Bellos, E., "The use of parabolic trough collectors for solar cooling—A case study for Athens climate", *Case Studies in Thermal Engineering*, Vol. 8, (2016), 403-413. (<https://doi.org/10.1016/j.csite.2016.10.003>).
28. Bergman, T.L., Incropera, F.P., DeWitt, D.P. and Lavine, A.S., *Fundamentals of heat and mass transfer*, John Wiley & Sons, (2011). (https://www.google.com/books/edition/Fundamentals_of_Heat_and_Mass_Transfer/vvyIoXEyWMoC?hl=en).
29. Ehyaei, M., Ahmadi, A., El Haj Assad, M., Hachicha, A. and Said, Z.J.S.E., "Energy, exergy and economic analyses for the selection of working fluid and metal oxide nanofluids in a parabolic trough collector", *Solar Energy*, Vol. 187, (2019), 175-184. (<https://doi.org/10.1016/j.solener.2019.05.046>).